LOODUSTEADUSKOND

Crustal thickness of Estonia: a receiver function analysis

Bachelor thesis

Student: Sonja Kõrvits
Student code: 206142LARB
Supervisor: Heidi Elisabet Soosalu, TalTech, Senior Lecturer, PhD
Co-supervisor: Argo Jõeleht, TU, Associate Professor in Geology, PhD
Study programme: Earth Systems, Climate and Technologies (LARB)

Tallinn 2025

Autorideklaratsioon

Kinnitan, et olen koostanud antud lõputöö iseseisvalt ning seda ei ole kellegi teise poolt varem kaitsmisele esitatud. Kõik töö koostamisel kasutatud teiste autorite tööd, olulised seisukohad, kirjandusallikatest ja mujalt pärinevad andmed on töös viidatud.

Autor: Sonja Kõrvits
[allkirjastatud digitaalselt]
28.05.2025

Töö vastab bakalaureusetööle esitatavatele nõuetele.
Juhendaja: Heidi Elisabeth Soosalu
[allkirjastatud digitaalselt]
28.05.2025

Table of contents

Abstract 3
Annotatsioon 4
List of figures 5
List of tables 6
1. Introduction 7
2. Basic Seismology 8
2.1. Structure of the Earth 8
2.2. The thickness of Earth's crust beneath Estonia 9
2.3. Seismic waves 9
2.4. Wave refraction and reflection 10
2.5. Wave velocity 11
2.6. Deconvolution 11
3. Receiver function method 13
4. Methods 14
4.1. Seismic stations 14
4.1.1. Estonian stations 14
4.1.2. International stations 14
4.2. Event selection 15
4.3. Software packages 16
4.4. Data Processing 16
5. Results 17
5. Discussion 23
Conclusions 25
Acknowledgements 26
References 27
Appendices 31
Appendix 1. The used seismic stations 31
Appendix 2. RF figures of SRGE and TOSE 32

Abstract

Relatively little research has been conducted on the thickness of the Earth's crust beneath Estonia and surrounding regions. Earlier studies, conducted in the late 1990s and early 2000s, relied on gravimetric, magnetic, and limited deep seismic sounding (DSS) data, often giving inconsistent results. In recent years, the expansion of the Estonian seismic network has given new opportunities for seismological interpretations.

For this study, seismic data of distant earthquakes from 12 Estonian and 5 nearby regional seismic stations were analysed using receiver function (RF) analysis. The methodology is based on the time delay between the arrival of direct pressure or P-wave and the converted Ps phase, where the P-wave is transformed into a shear or S-wave at an interface. This time difference allows for the estimation of the depth of Moho, the boundary between Earth's crust and mantle. Most of the analysis was conducted using the PyGLImER software package.

The results reveal significant variation in Moho depth, ranging from 48 km in southeast Estonia to 63 km in the northwest. The findings are broadly consistent with the existing DSS profile and regional gravity anomalies.

The main limitation of this study is the sparse station coverage in southern Estonia and Latvia, which affects reliability of the results in these areas. Nevertheless, the results demonstrate that receiver function analysis is a plausible and effective method for crustal studies in the Estonian region. The findings provide valuable insight into the crust beneath Estonia, and offer basis for future studies that combine seismological, gravity, and other geophysical data.

Eesti maakoore paksus: vastuvõtjafunktsiooni analüüs

Annotatsioon

Eesti maakoore paksust on seni uuritud suhteliselt vähe. Varasemad uuringud, mis on tehtud peamiselt 1990. aastate lõpus ja 2000. alguses, tuginesid ainult gravimeetrilistele, magnetilistele ning süvaseismilistele andmetele, andes sageli erinevaid tulemusi. Viimastel aastatel on Eesti seismojaamade võrk oluliselt laienenud, mis pakub võimalust ka maakoore seismoloogilisteks tõlgendusteks.

Käesolevas töös analüüsiti kaugete maavärinate seismilisi andmeid 12 Eesti ja viie lähiriikides asuvast seismojaamast, kasutades vastuvõtjafunktsioonide analüüsi. Meetod põhineb piki- ehk P-laine ja mõnel piirpinnal tekkinud muundunud Ps-laine (pikilaine muundus rist- ehk S-laineks) faasi vahele jääval ajal. Selle ajavahe põhjal on võimalik hinnata Moho pinna ehk Maa koore ja vahevöö vahelise eralduspinna sügavust. Analüüs viidi läbi PyGLImER tarkvarapaketi abil.

Tulemused näitavad suurt Moho sügavuse erinevust Eesti aladel. Kõige väiksem on maakoore paksus Kagu-Eestis – 48 km, ning kõige suurem Loode-Eestis, ulatudes 63 km-ni. Leitud sügavused on üldjoontes kooskõlas süvaseismika ning gravitatsioonianomaalia andmetega.

Analüüsi piirab peamiselt seismojaamade hõre jaotus Lõuna-Eestis ja Lätis. See vähendab nende piirkondade tulemuste usaldusväärsust. Siiski näitavad tulemused, et vastuvõtjafunktsioon on usaldusväärne ja sobiv meetod maakoore ehituse uurimiseks Eesti aladel. Töö pakub uusi teadmisi Eesti maakoore paksuse kohta ning loob aluse tulevastele Maa siseehituse uuringutele.

List of figures

Figure 1. Earth's inner structure.

Figure 2. Propagation of body waves as function of particle motions.

Figure 3. A schematic diagram of reflected and refracted waves generated from an incident P-wave.

Figure 4. Schematic ray paths for different labelled phases and multiples from a simple two-layer model with the resultant radial receiver function.

Figure 5. Seismic stations used in this study.

Figure 6. Receiver functions and estimated Moho depth: A) NOPE; B) MTSE; C) EE06; D) PLDE.

Figure 7. Receiver functions and estimated Moho depth: A) SRPE; B) ARBE; C) EE04; D) PUL.

Figure 8. Receiver functions and estimated Moho depth: A) PISE, automatic result; B) PISE my interpretation; C) VSU; D) TRTE.

Figure 9. Receiver functions and estimated Moho depth: A) MEF; B) PVF; C) VJF; D) SLIT.

Figure 10. Interpolated Moho depth map beneath Estonia and surrounding regions based on receiver function analysis.

Figure 11. Sovetsk–Kohtla-Järve seismic sounding (DSS) profile and gravity profile. Moho depths from Ankudinov et al. (1994), All et al. (2004) and this study.

Figure 12. A) Filtered gravity data of Estonia and its surrounding areas. B) Bouguer gravity map of Estonia.

List of tables

Table 1. Velocity model used in this study.

Table 2. Overview of seismogram data and RF extraction.

1. Introduction

Relatively little research has been conducted on the thickness of the Earth's crust beneath Estonia. While several studies emerged in the late 1990s and early 2000s, this topic has received limited attention over the last two decades. Most existing studies rely on gravity and magnetic data, which have produced highly varying interpretations. One geophysical method that has remained largely unexplored in Estonia is seismology.

In recent decades, receiver function analysis has become a widely used seismic method for imaging Earth's internal discontinuities, such as the Mohorovičić discontinuity (Moho). This technique uses distant earthquake P-waves, which are converted to S-waves at boundaries with strong velocity contrasts. These converted waves, recorded by seismometers, provide detailed information, particularly on the depth and character of the Moho. The receiver function analysis method has been applied all over the world. However, its application in the Baltic region has so far been limited, primarily due to a small number of seismic stations.

Until now, the only published seismic information about the deep crust in Estonia came from Sovetsk–Kohtla-Järve profiles deep seismic sounding (DSS) studies by Ankudinov et al. (1994), which was later used by All et al. (2004) to create a map of crustal thickness. In recent years the Estonian seismic station network has expanded considerably. Thus, it is now possible to use receiver function analysis with enough detail to study the structure of the crust.

This thesis uses receiver function analysis to investigate the crustal thickness beneath the entire territory of Estonia for the first time. Waveform data were collected from Estonian seismic stations and supplemented by five stations in surrounding regions to ensure full national coverage. The goal is to produce a reliable estimate of the Moho depth across the country. This study provides a new seismic perspective on the crust beneath Estonia.

2. Basic Seismology

Seismology studies how acoustic waves travel through the Earth. Strong earthquakes generate pressure waves, which act as natural sources of seismic energy, these waves travel through the Earth and are detected by seismographs (receivers) on the other side (Mondol, 2010).

2.1. Structure of the Earth

The Earth is made up of layers that can be described in two main ways: by their composition (crust, mantle, and core) and by their rheological properties (Figure 1). Rheologically, the outer layer is lithosphere, which includes the crust and the upper rigid part of the mantle. Beneath the lithosphere lies the asthenosphere, a viscous, ductile layer. Transitions between these layers are marked by discontinuities.

For the receiver function method the most important boundary is the Mohorovičić or Moho discontinuity, which is named after the Croatian seismologist Andrija Mohorovičić, who discovered it in 1909 (Mohorovičić, 1910). The Moho separates the Earth´s crust from the mantle. These two layers are composed of different types of rocks: the crust mainly consists of felsic and mafic rocks, while the mantle consists of ultramafic rocks (Kaban et al., 2022). As a result, seismic waves propagate at different speeds through each layer. The depth of the Moho varies: it ranges from 5 to 10 km below the ocean floor and from 20 to 90 km beneath continents (He et al., 2018; Shearer, 1999).

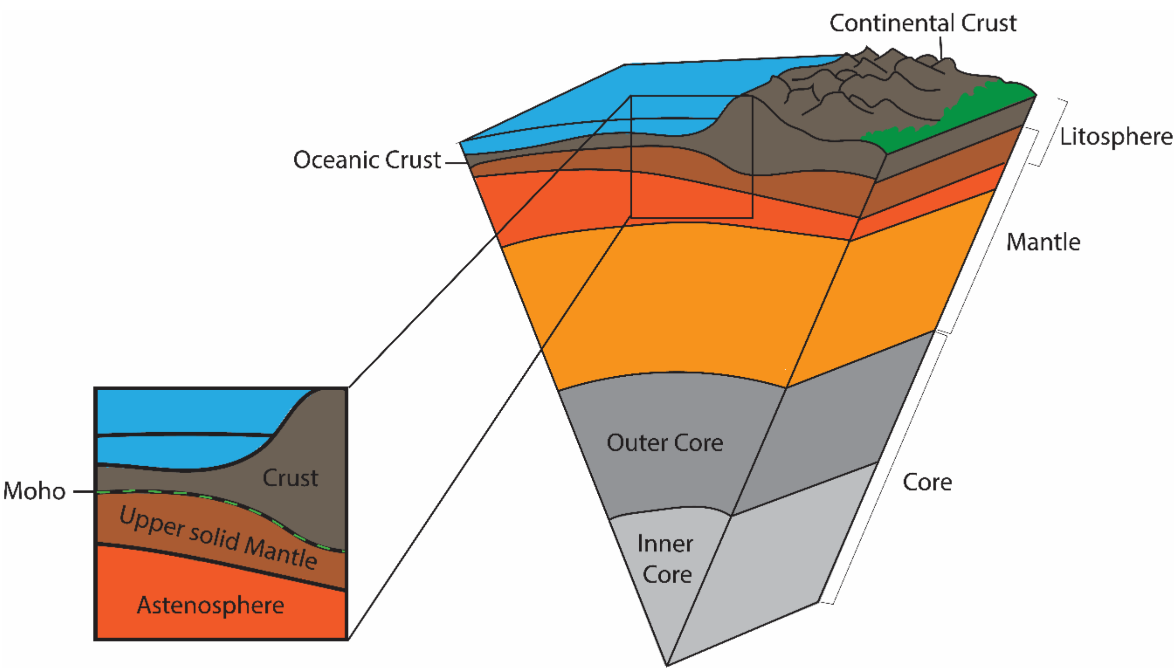

Figure 1. Earth’s inner structure.

2.2. The thickness of Earth's crust beneath Estonia

Relatively little research has been conducted on the thickness of the crust beneath Estonia. The first important study was carried out by Ankudinov et al. (1994), which was the Sovetsk—Kohtla-Järve deep sounding profile. This work laid the foundation for many later studies. The first map showing crustal thickness in Estonia was produced by Sildvee and Vaher (1995), who estimated that the thickness ranges from 35 to 50 km. A more detailed and updated map was later developed by All et al. (2004), incorporating quantitative gravity and magnetic modelling. Their results suggest that the crust in Estonia is overthickened, reaching depths of approximately 45 to 65 km. The most recent study by Solano-Acosta et al. (2023) suggests even greater depths of 48.6 to 72.9 km based on gravity data alone.

Grad et al., (2009) produced the first high-resolution model of the Moho depth of the European Plate by combining receiver function analysis and seismic and gravity data. Their work indicates that the depth of the Moho lies under 50 km in eastern Estonia, but it may reach as much as 60 km in southern Estonia. However, they note that the depth uncertainty of the Estonian Moho may be more than 5 km.

2.3. Seismic waves

For a three-component seismic station, the velocity of ground movements is measured and recorded in three directions: vertical (Z), north-south (N) and east-west (E) – one vertical and two perpendicular horizontal motions. The faster of the two types of body waves is known as the primary, pressure or P-wave (for the theory of propagation of seismic waves, see e.g., Bolt, 2003; Ravikumar et al., 2014; Shearer, 1999). P-waves propagate through rock by causing alternating compression and expansion in the direction they travel. The slower body wave is called secondary, shear or S-wave, which travels by shearing the rock sideways, perpendicular to its propagation direction (Figure 2). The perpendicular displacement cannot occur within fluids, so S-waves can only travel through solid material. P-waves are most prominently recorded on the vertical motion component of seismograms, while S-waves are more noticeable on the horizontal components. S-waves are the main cause of structural damage due to their shearing motion and larger amplitude.

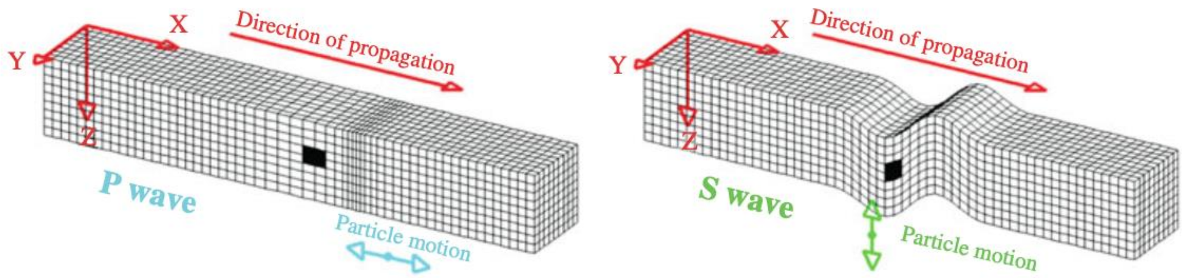

Figure 2. Propagation of body waves as function of particle motions (Mondol, 2010).

The velocity of seismic waves depends on the composition, density and elastic properties of the rocks and materials they pass through. The first noticeable motion of a seismic wave on a seismogram is called its arrival time. The time differences between P- and S-waves are used to determine the location of an earthquake.

Measuring the arrival times of seismic waves at different distances between the earthquake location and receivers, seismologists can create travel-time curves. These curves help interpreting Earth´s average velocity structure.

2.4. Wave refraction and reflection

The two body waves, P and S have another characteristic that affects shaking: when they propagate through layers of rock, they are reflected and/or refracted at the boundary between rock types. Seismic ray theory is analogous to optical ray theory and has been applied for over 100 years to interpret seismic data (Shearer, 1999).

Reflection occurs as it is formulated by the law of reflection – the angle of reflection is equal to the angle of incidence. In this study, the analysis primarily relies on seismic refraction. Refraction behaves according to the law of refraction, or Snell's law – when light travels from one medium to another, it changes propagation direction (e.g., Born & Wolf, 1959)

$$\frac{\sin(\theta_1)}{V_1} = \frac{\sin(\theta_2)}{V_2}$$

where indices 1 and 2 are referring to different medias, θ shows the angles of incidence and refraction, and V shows velocities of the different layers.

In addition to normal refraction and reflection, seismic energy is also redistributed into other types of waves. An incident P-wave creates both reflected and refracted P- and S-waves when it encounters a boundary between rock types (Bolt, 2003) (Figure 3). For example, as a P-wave travels upward through the mantle and strikes the Moho discontinuity, most of its energy continues as a transmitted P-wave, while a portion is converted and transmitted as an S-wave. These waves are observed at seismic stations as distinct signals, specifically the direct P-wave and the Ps-wave.

The redistribution of seismic energy at such boundaries is mathematically described by the Zoeppritz equations (Shuey, 1985). Zoeppritz equations are a set of equations that describe the partitioning of seismic wave energy at the interface ("Zoeppritz equations", 2024). Thus, it is important to note that the first recorded S-wave signal during distant seismic events, such as earthquakes, is not the original S-wave but rather the converted Ps-wave (Shuey, 1985). In this study, the focus is not on the specific distribution of directions and strengths of these waves, but on the fact that such redistribution occurs.

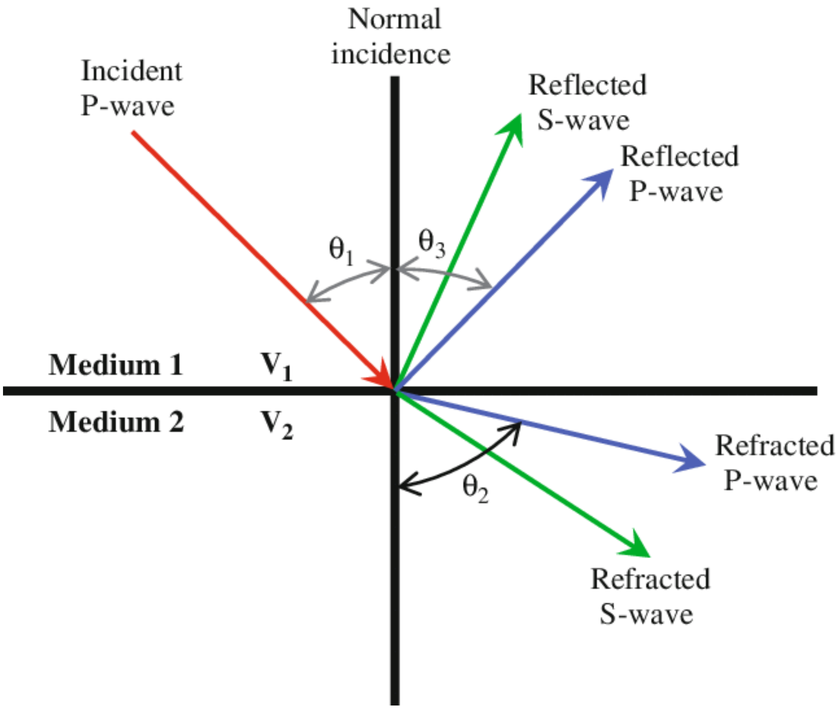

Figure 3. A schematic diagram of reflected and refracted waves generated from an incident P-wave (Mondol, 2010).

2.5. Wave velocity

Seismic velocity generally increases with depth, primarily due to compaction of the material. However, lithologic changes introduce low-velocity zones, where seismic velocity decreases locally due to changes in rock type, porosity, or fluid content (Bormann et al., 2012). At discontinuities, the increase in velocity can be nearly instantaneous (Bormann et al., 2012).

The average crustal P-wave velocity is about 6.5 km/s (Christensen & Mooney, 1995). S-wave velocities are generally about 60% of P-wave velocity, depending on the rock type (Christensen & Mooney, 1995; Tiira, et al., 2022). With known seismic velocities, the Moho depth can be calculated using the formula:

$$H = t_{Ps} \times \left(\frac{V_p \times V_s}{\sqrt{V_p^2 - V_s^2}} \right)$$

where H is the depth to the Moho, t_{Ps} is the time difference between the direct P-wave and the converted Ps-wave arrival, V_p is the P-wave velocity and V_s is the S-wave velocity.

2.6. Deconvolution

In general, any measured signal will contain some noise due to various physical factors. Noise affects the accuracy of the measurement, so it is important to minimize it. This can be achieved through methods such as frequency filtering or selecting signals with inherently low noise levels

(Castro-Artola et al., 2022). A common technique to enhance signal quality is deconvolution (Chen et al., 2024). Deconvolution compresses wavelets in the seismogram, which increases resolution and mitigates noise (Chen et al., 2024; Backus et al., 2001).

Large-magnitude earthquakes typically generate signals that are less affected by noise compared to smaller events (Matcharashvili et al., 2012). Consequently, a higher signal-to-noise ratio (SNR) is generally observed for large-magnitude earthquakes, making them more suitable for analysis (Chen et al., 2024). Additionally, as a seismic signal propagates, its strength gets weaker further away, reducing the SNR (Chen et al., 2024). The magnitude of an earthquake is strongly correlated with the average SNR, emphasizing its significance in selecting data for analysis. The SNR in seismic data is higher when waves propagate through hard rock compared to sedimentary layers; this is due to physical properties of the materials.

3. Receiver function method

A receiver function (RF) is a tool used in seismology to study the internal layers of the Earth. It was originally developed by Langston (1979) but has been improved by many others since (Saygin, 2007). It is mostly used for measuring the thickness of the Earth's crust (Akinremi et al., 2024). The velocity contrast at the Moho represents a major discontinuity to which RFs are highly sensitive (Akinremi et al., 2024). It is a widely used technique because it can be applied using passive data (recordings) and requires only a single seismic station.

Receiver functions are time series, computed from three-component seismograms, capturing the Earth's structural response near the seismic receiver. These responses originate from the different paths travelled by waveforms generated by distant earthquakes, known as teleseismic waves. As S-waves travel slower than P-waves, they arrive at seismic stations later, after the initial P-wave. But as said before, both waves reflect and refract, and get converted into Ps, PpPp, PpPs, PpSs etc. (in general, a capital letter denotes a refracted wave, and a lowercase letter denotes a reflected wave) (Figure 4). The time difference between the arrival of the direct P-wave and the converted Ps phase (where the P-wave transforms into an S-wave at an interface) allows for a direct calculation of the Moho's depth (Delph et al., 2019). The result is a time series called the RF, which contains converted seismic phases created at boundaries inside the Earth. For this method, the RF is only watched from the moment a wave has converted from Moho to the time it has reached the station. However, the presence of low-velocity sedimentary layers can obscure Moho signals, as these layers create additional wave conversions that complicate the RF (Akinremi et al., 2024). In Estonia the sedimentary cover is relatively thin (200–500 m), so it should not affect the results in this study.

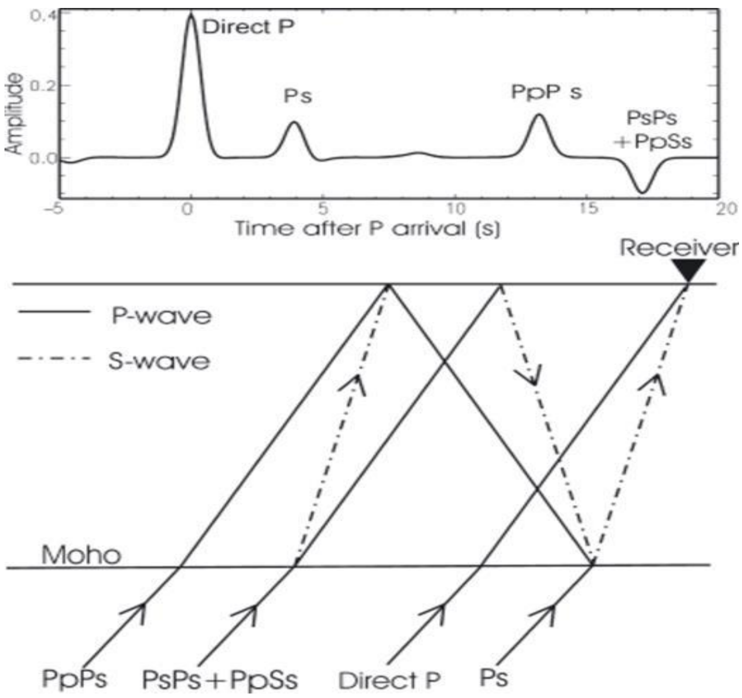

Figure 4. Schematic ray paths for different labelled phases and multiples from a simple two-layer model with the resultant radial receiver function (Harland et al., 2009).

4. Methods

4.1. Seismic stations

In this study, I use data from twelve Estonian, three Finnish, one Latvian and one Russian seismic station (Figure 5) (Appendix 1). For Estonia I included all available seismic stations listed in the GEOFON database. The additional stations were selected based on their locations to cover as large area of Estonia as the seismic network allows. All the stations are part of GEOFON Seismic Network (GEOFON Data Centre, 1993).

4.1.1. Estonian stations

There are three seismic stations located in western Estonia (for information about the Estonian Seismic Network, see e.g., EGT, 1996; Soosalu, 2024). The Matsalu (MTSE) station is located in a separate cellar at the Matsalu Nature Park Centre and has been in operation since 2006. EE06 is a temporary station in Hiiumaa, installed in 2015. Additionally, the NOPE station is located in Peraküla, Nõva commune.

In northern Estonia there are four stations. The newest Estonian station is PLDE, which started operating in the summer of 2024. It is located in Paldiski and its site is very close to the Suurupi station (SRPE), which operated from 2005 to 2011. The Arbavere (ARBE) station has been active since 2011 and is located at the Arbavere Research Centre of the Geological Survey of Estonia. EE04 is a temporary station installed in May 2015 in the Vaivara Sinimägede area near Narva-Jõesuu. Although the site is affected by high-frequency noise from an ambient air quality monitoring station operated by the company Eesti Energia, the noise does not interfere with the low-frequency teleseismic signals required for RF studies.

The remaining stations are located in central and southern Estonia. Särghaua (SRGE), and Tooma (TOSE) are both relatively new stations, installed in 2023. TOSE previously operated as a temporary station under the name EE03 However, in this study, only data from the upgraded TOSE are used. The sites of Vasula (VSU) and Tartu (TRTE) stations are located very near to each other. The Tartu station was active from 1996 to 2003 at the Tartu Old Observatory. Approximately 10 km to the north there is Vasula station, which has been operating since 2003. The Piusa seismic station, originally named as EE07, has been located in the Piusa caves from May 2017. In 2023, the temporary station was replaced by a permanent one and was renamed as PISE. In this study only data from PISE are used.

All Estonian stations are equipped with broadband seismometers – Güralp CMG-6T, Nanometrics Trillium Compact Horizon or Streckeisen STS-2 (Soosalu, 2025). These are low-noise seismometers with an extended low-frequency sensitivity (Nanometrics Inc, 2009), making them useful for large distant teleseismic wave observations, needed for RF studies.

4.1.2. International stations

The Finnish seismic stations used in this study are all located in southern part of the country (for the information about Finnish Seismic Network, see e.g., Institute of Seismology, University of Helsinki, 1980). The Metsähovi (MEF) station, located near Espoo, has been in operation since 2006.

Approximately 100 km to the east is a Pernaja (PVF) station. The station has been active since 1991. Near the Finland – Russia border is a station Virolahti (VJF), which has been working since 2006.

Slitere (SLIT) station is located near Ventspils and has been working since 2006. This station is particularly useful for seismic studies in Estonia, because there are no seismometers in the Saaremaa Island. In Russia, the Pulkovo (PUL) station, located in Saint Petersburg, has been in operation since 1998.

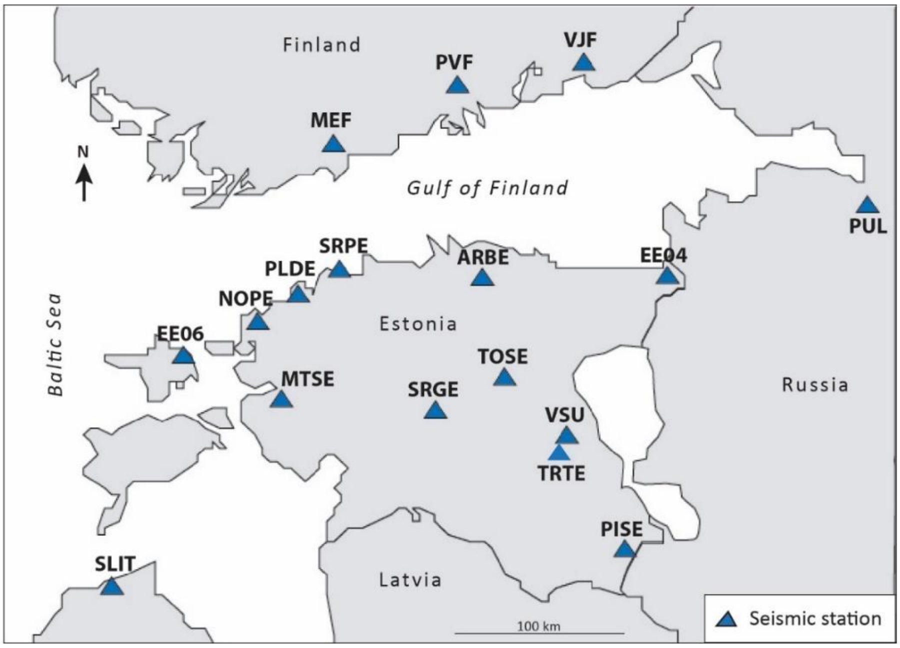

Figure 5. Seismic stations used in this study.

4.2. Event selection

Tšugai (2010) carried out a preparatory analysis for identifying seismic regions suitable for RF analysis in Estonian. As the theory defines, she outlined the potential data set within the 30–90 degree epicentral distance from Estonia, including earthquakes with a magnitude at least 5.5 and SNR greater than 20 dB. The same parameters were used in Aedma (2020) work, where he used RF method for Vasula (VSU) station.

I downloaded all the raw waveforms from Potsdam GEOFON archive, which provides access to seismic waveform data from global network stations (e.g., Quinteros et al., 2021a). GEOFON itself operates a global seismic network, through which I was able to obtain data from Russian and Latvian seismic stations. The downloaded data file format is the widely used MiniSEED (e.g., Ringler & Evans, 2015; Quinteros, 2021b).

Initially, I planned to pre-filter and download only events with a magnitude greater than 6.5. However, this approach resulted in a very small dataset. I expanded the selection criteria to include earthquakes with magnitude 5.5 for stations that began distributing their data to GEOFON in 2023 or later. This adjustment provided me with a much larger dataset, consisting of 200–400 seismograms, which was more suitable for further analysis.

4.3. Software packages

The main packages used in this study were PyGLImER, ObsPy and NumPy, all of which are Python-based. PyGLImER is a framework for "Global Lithospheric Imaging using Earthquake Recordings" (GLImER), which automates RF processing – from downloading data to imaging (Makus et al., 2021). It is built largely on the ObsPy project, which is broader seismological data processing framework (e.g., Beyreuther et al., 2010). NumPy is a widely used numerical library that provides support for efficient operations on matrices and multi-dimensional arrays (Harris et al., 2020).

The PyGLImER software was last updated in 2023. However, updates to NumPy and ObsPy caused compatibility issues, making it difficult to get everything work together. After resolving these issues, I was able to successfully match the required versions to ensure full functionality: Python 3.9.6, PyGLImER 0.4.1, ObsPy 1.3.1, and NumPy 1.25.2.

4.4. Data Processing

After downloading the raw waveform data from the GEOFON archive, I began preprocessing the data. The first step was to clip each waveform to the appropriate length. This was followed by demeaning and detrending the waveforms to remove any offset and linear trend, which helps stabilise the data. Then I removed the instrument response and converted the data to velocity. The waveforms were then rotated from the original ZNE (vertical, north, east) components to NEZ. However, in this coordinate system, the data is not aligned along the axis between the station and earthquake. Therefore, a two-dimensional rotation is applied to get RTZ (radial, transverse, vertical) components, which is the preferred system for RF analysis. Once the waveforms were in RTZ format, I applied the SNR filter, that it would be greater than 20 dB. The final step in preprocessing was deconvolution. This step produced the final RFs used in analysis (Table 2).

After the RFs were computed, they were plotted and stacked to create an average waveform for each station. The RFs were stacked by aligning the P-wave arrival times, so that reflections from Moho would align as well. From the stacked RFs I calculated the Moho depth. For this purpose, I employed a seismic velocity model developed at the Institute of Seismology, University of Helsinki (e.g., Tiira et al., 2022) (Table 1), since there is no Vp/Vs seismic velocity model for Estonia.

Table 1. Velocity model used in this study.

Vp (km/s)	**Vs (km/s)**	**Depth range**
6.19	3.6	0—15 km
6.7	3.84	15—40 km
8.03	4.64	> 40 km

5. Results

The Tartu (TRTE) and Pulkovo (PUL) stations had the least usable data, with only 30 and 15 seismograms, respectively, resulting in just 5 usable RFs. For Pulkovo, this limitation might be due to the station not having accessible data to download since 2001. The smaller amount of data from Tartu is less of a concern, as it primarily serves as a control station for Vasula, given their proximity to each other.

Overall, approximately every second waveform was suitable for RF analysis (Table 2). The primary reason for waveform rejection was a low signal-to-noise ratio. Among the Estonian stations, NOPE and VSU produced the highest quality RFs. The Finnish stations also provided excellent data quality, likely due to their location on hard igneous bedrock, which produces lower ambient noise because of reduced wave scattering and surface interference.

Table 2. Overview of seismogram data and RF extraction.

Station name	Measurement period used	Minimum magnitudes	No. of downloaded seismograms	No. of RF-s
ARBE	2011.01.20 - 2024.04.17	5.5	767	352
EE04	2023.10.18 - 2025.04.10	5.5	255	86
EE06	2023.10.18 - 2025.04.17	5.5	275	131
MEF	2011.02.15 - 2025.04.17	6.5	237	126
MTSE	2006.01.01 - 2024.07.01	6.5	891	235
NOPE	2023.10.18 - 2025.04.14	5.5	277	156
PISE	2023.10.18 - 2025.04.17	5.5	279	137
PLDE	2024.10.30 - 2025.04.24	5.5	96	26
PUL	1998.01.01 - 2010.04.22	5.5	16	5
PVF	2018.04.19 - 2025.04.24	6	399	195
SLIT	2006.10.25 - 2024.04.17	6.5	351	172
SRGE	2023.10.18 - 2025.04.17	5.5	280	143
SRPE	2005.03.22 - 2011.01.03	6.5	142	76
TOSE	2023.10.18 - 2025.04.17	5.5	276	150
TRTE	1996.10.18 - 2003.04.26	6.5	30	5
VJF	2011.02.15 - 2025.04.17	6.5	390	311
VSU	2003.04.12 - 2025.04.10	6.5	308	249

Most analysed stations provided reliable and well-defined receiver functions. For better visualisation of the RFs, positive amplitudes are shown in red and negative amplitudes in blue. A clear Moho signal is seen at the NOPE station in Nõva, where the stacked RF reveals a distinct arrival, indicating that the Moho lies at approximately 63 km depth (Figure 6A). At the Matsalu (MTSE) station, which provided over 200 usable RFs, the signal is similarly strong, suggesting a Moho depth around 61 km (Figure 6B). EE06 in the Hiiumaa island, also showed high-quality RFs, which the Moho depth is interpreted to be about 60 km (Figure 6C).

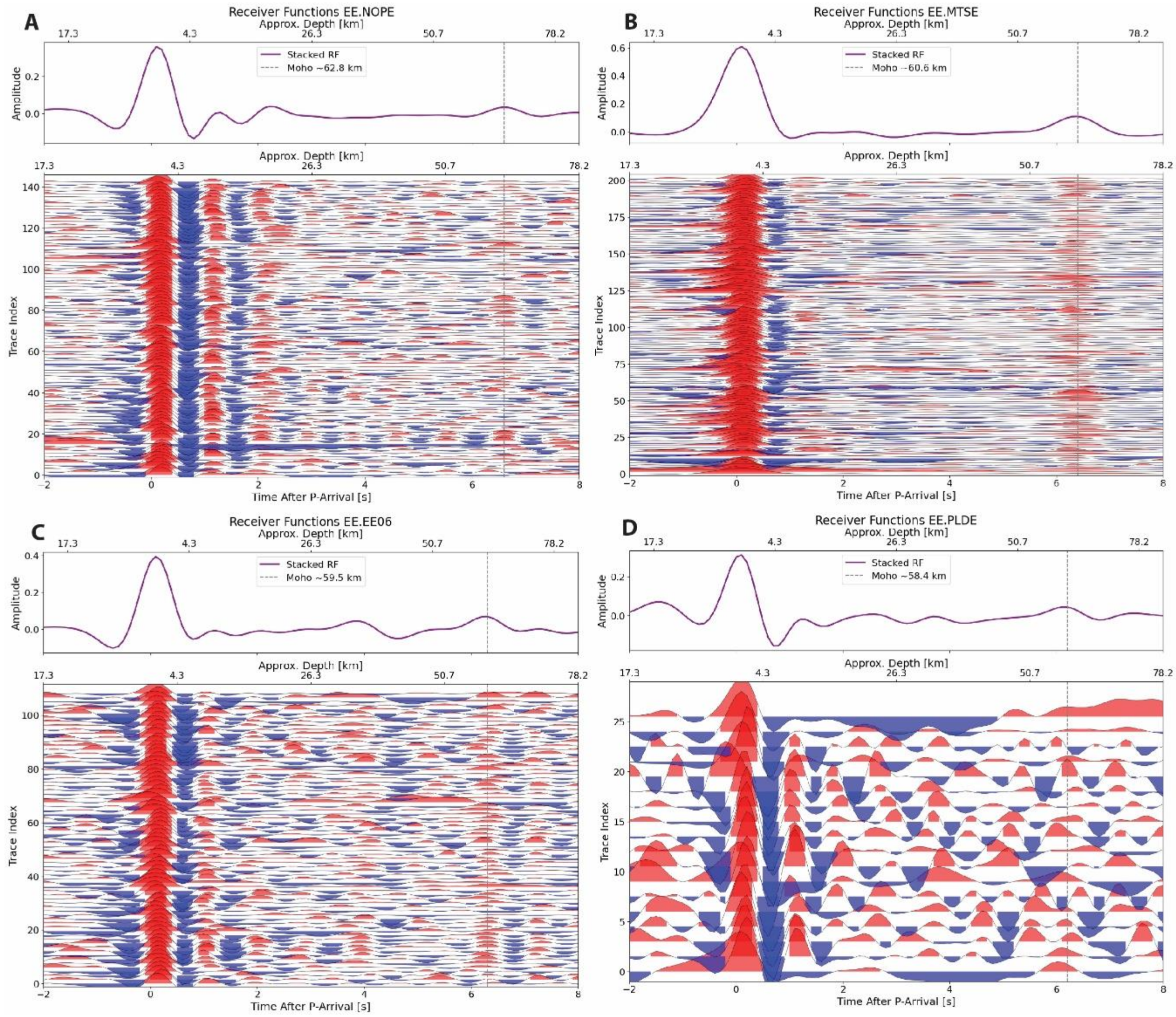

Figure 6. Receiver functions and estimated Moho depth. The panels show individual (below) and stacked (above) RFs. The dashed line marks the interpreted Moho Ps arrival. Stations: A) NOPE; B) MTSE; C) EE06; D) PLDE.

Stations in north-western Estonia produced consistent results. Paldiski (PLDE), the newest among them, is located at the transition zone between deeper Moho in the east and the shallower crust beneath northern Estonia. PLDE had fewer usable events than nearby stations, so the result is less certain. The Ps phase arrives just after 6 seconds, meaning a Moho depth of 58 km, which fits the regional trend (Figure 6D). Suurupi (SRPE) showed a weaker signal with higher uncertainty. The stacked RF suggests a depth of about 53 km, although by visual inspection I would place it closer to 54–55 km (Figure 7A). The RFs at SRPE appeared particularly noisy.

Arbavere (ARBE) produced the highest number of usable RFs. A comparison between stacks using 100 and 300 RFs showed no difference in the result, indicating the station's overall high data quality. The Moho beneath ARBE is located at approximately 54 km (Figure 7B). At EE04 in Vaivara, the RFs are quite noisy, yet the Moho is clearly visible at 55 km (Figure 7C). Interestingly, the same waveform pattern appears at the Russian PUL station in Saint Petersburg, where the Moho is estimated at around 64 km (Figure 7D). However, only five usable RFs were available from PUL and thus uncertainty is high.

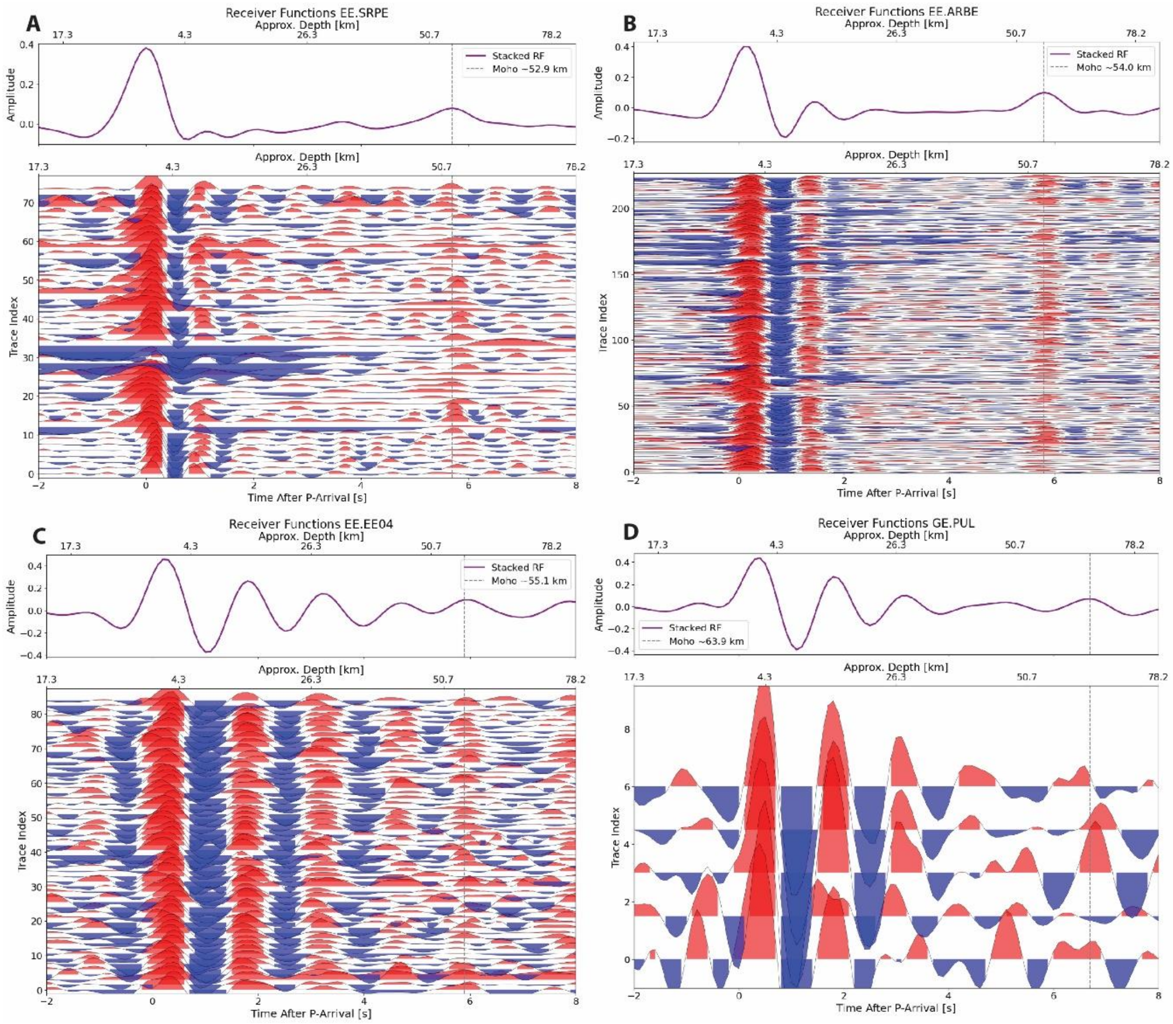

Figure 7. Receiver functions and estimated Moho depth. The panels show individual (below) and stacked (above) RFs. The dashed line marks the interpreted Moho Ps arrival. Stations: A) SRPE; B) ARBE; C) EE04 ; D) PUL.

In southern and central Estonia, the Särghaua (SRGE) station produced clean and distinct signals, with a Moho depth of approximately 54 km (Appendix 2). The Tooma (TOSE) station also gave a substantial number of RFs, suggesting a Moho at 53 km. However, visual inspection of the stacked graph indicates the depth could be closer to 54–55 km (Appendix 2). A notable result was obtained at Vasula (VSU), where the Moho appears significantly shallower than at the other stations, approximately 48 km (Figure 8C). This observation was supported by data from the nearby Tartu station (TRTE), where the Moho depth was measured at 49 km (Figure 8D). The motivation to include TRTE was mostly as a control for Vasula due to their proximity.

The station Piusa (PISE) produced the most uncertain result. The automatic calculation placed the Moho at a depth of about 69 km, but visual analysis of the RFs suggests that the converted phase arrives closer to 6.7 seconds, corresponding to a Moho depth of approximately 60 km (Figure 8A, B).

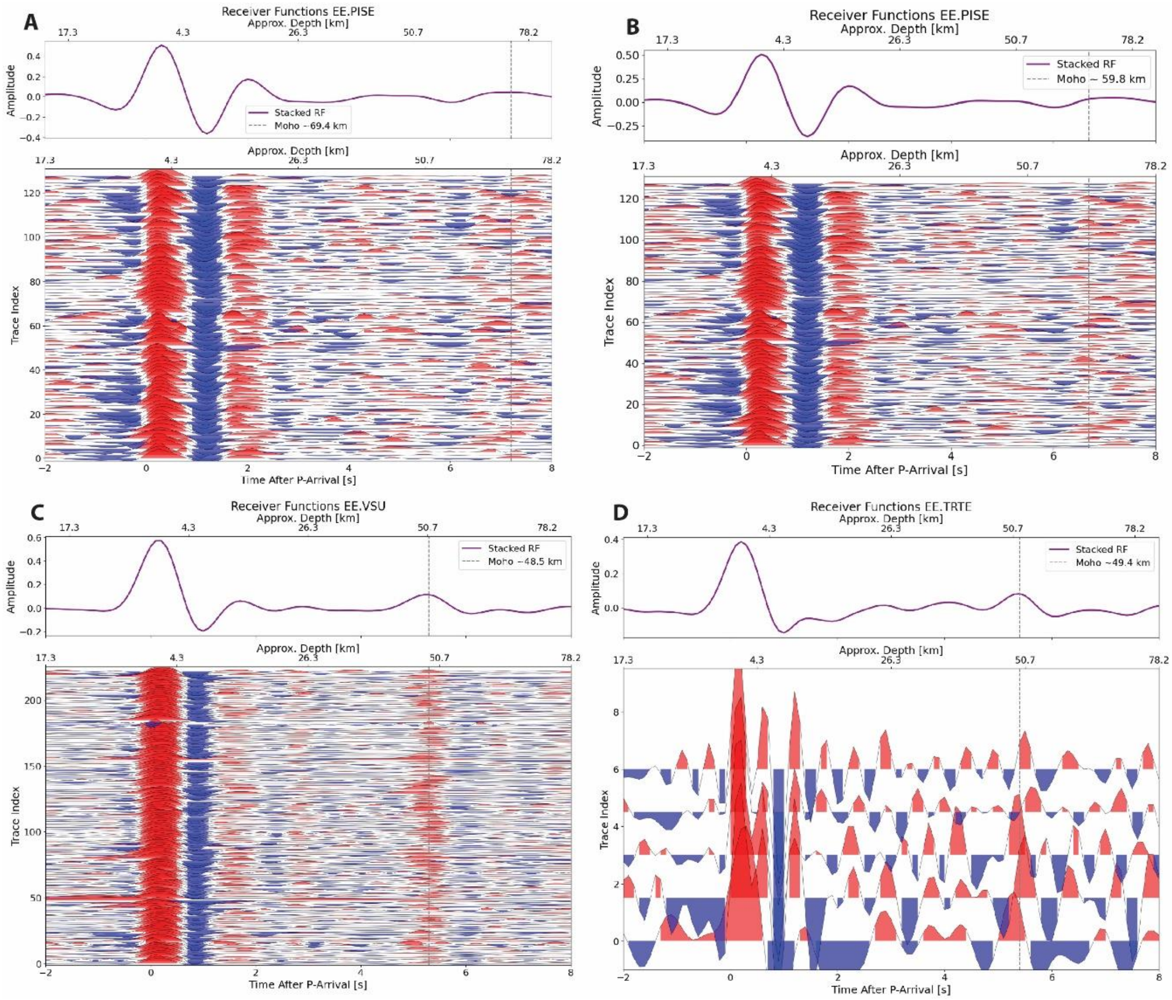

Figure 8. Receiver functions and estimated Moho depth. The panels show individual (below) and stacked (above) RFs. The dashed line marks the interpreted Moho Ps arrival. Stations: A) PISE, automatic result; B) PISE my interpretation; C) VSU; D) TRTE.

The Finnish stations all yielded high-quality RFs. At MEF, near Espoo, the Moho lies at around 56 km (Figure 9A). At PVF, it is approximately 49 km (Figure 9B), and at VJF, near the border between Finland and Russia, about 50 km (Figure 9C). In contrast, the Latvian station SLIT, with relatively noisy signal, had a very clear Moho signal at 45 km (Figure 9D).

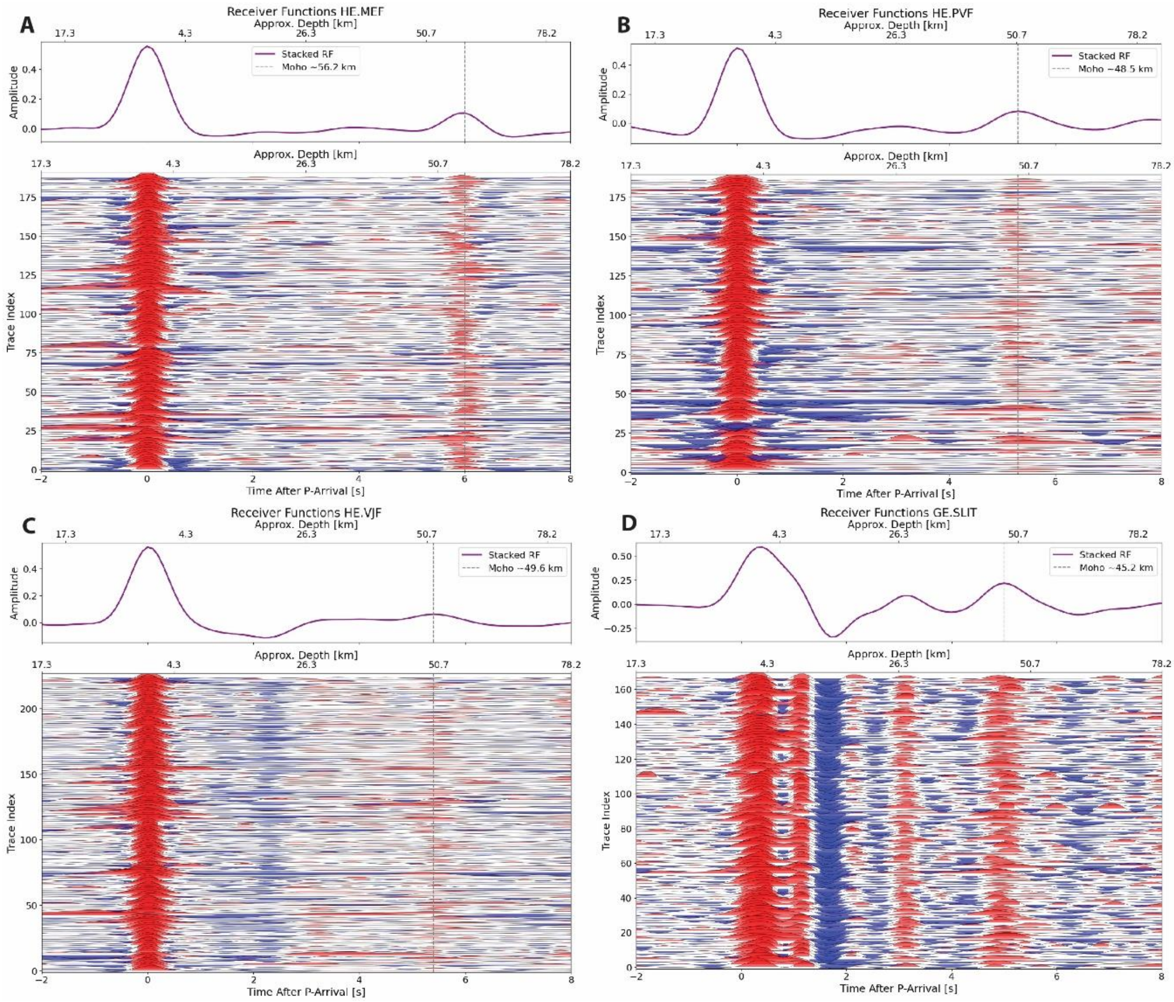

Figure 9. Receiver functions and estimated Moho depth. The panels show individual (below) and stacked (above) RFs. The dashed line marks the interpreted Moho Ps arrival. Stations: A) MEF; B) PVF; C) VJF; D) SLIT.

Based on the interpreted Moho depths from all analysed stations, I constructed an interpolated Moho depth map of Estonia (Figure 10).

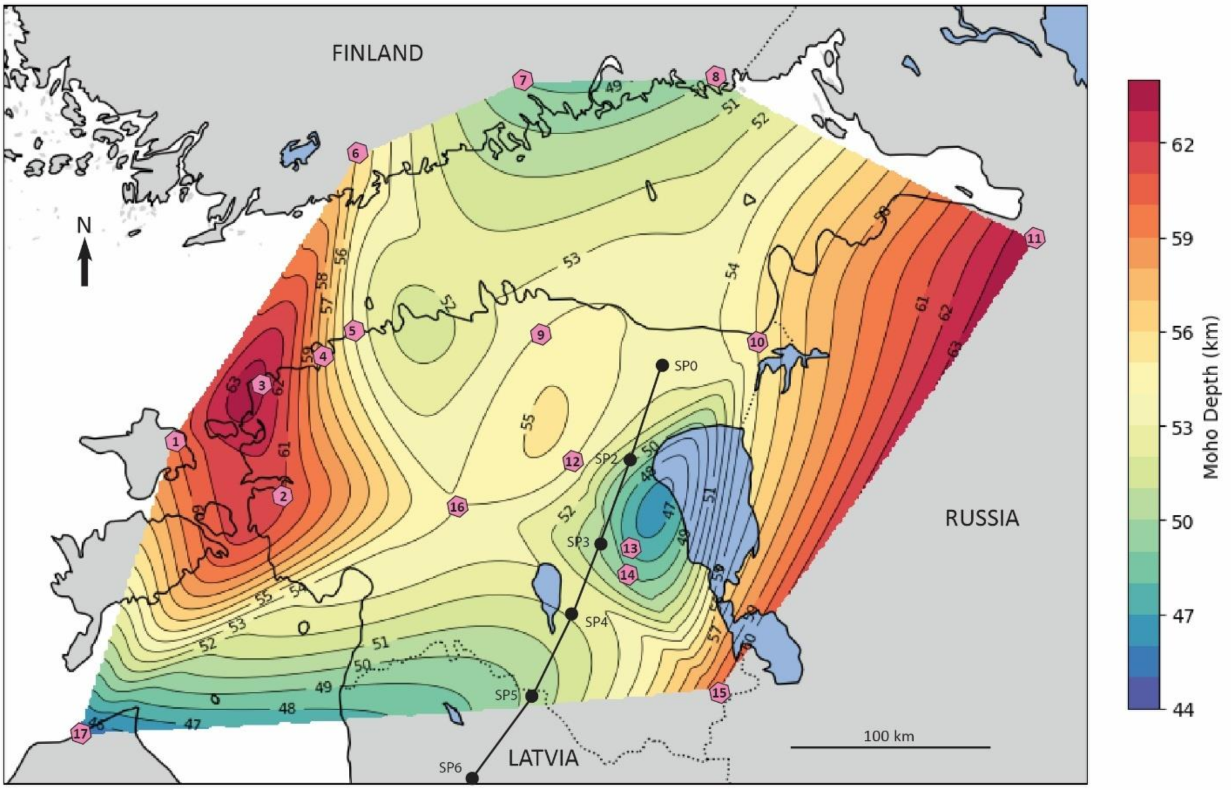

Figure 10. Interpolated Moho depth map beneath Estonia and surrounding regions based on receiver function analysis. The numbers in pink indicate seismic stations used in this study: 1) EE06; 2) MTSE; 3) NOPE; 4) PLDE; 5) SRPE; 6) MEF; 7) PVF; 8) VJF; 9) ARBE; 10) EE04; 11) PUL; 12) TOSE; 13) VSU; 14) TRTE; 15) PISE; 16) SRGE; 17) SLIT. The black line marks the location of the Sovetsk—Kohtla-Järve deep seismic sounding (DSS) profile.

5. Discussion

The results of this study are limited by the sparse distribution of seismic stations, which makes direct comparisons with existing knowledge challenging. With 12 stations in the country, plus five nearby stations, there are significant gaps between data points. This limitation is particularly evident in the southern Estonia and northern Latvia, where the SLIT station in Latvia is the only available source. Its data are not sufficient to fully constrain the regional Moho structure (e.g., Grad et al., 2009; Zandersons & Karušs, 2020). Expanding the seismic network in this region would significantly improve the accuracy and resolution of future models.

Despite the limitations of the seismic network, the findings align well with previous regional studies. The Moho depth beneath Vasula (VSU) was 48 km, closely matching Aedma's (2020) result of 47 km. The nearby Tartu (TRTE) station yielded a similar result of 49 km, further validating this observation. In northern Estonia, the stations produced consistent results, typically indicating Moho depths within 53–58 km. Initially, the deepest Moho was detected beneath the Piusa (PISE) station, however after evaluating the results more critically, I interpreted the Moho depth to be smaller. Consequently, the deepest Moho depth was under Nõva (NOPE) station (63 km), and the shallowest was at SLIT (45 km).

The best direct seismic comparison is the Sovetsk–Kohtla-Järve deep seismic sounding (DSS) profile, originally published by Ankudinov et al. (1994) and later modified by All et al. (2004) (Figure 11). Ankudinov et al. (1994) identified a transitional Moho boundary, marked by M1 and M2. My results fall within these depths. Unfortunately, there is no data from other publications between shot points SP2 and SP0 to compare with my results. Furthermore, the lack of seismic stations in southern Estonia and Latvia limits the reliability of my profile beyond SP5. Interestingly, my Moho depth profile shows better agreement with the gravity profile trend than the other seismic models.

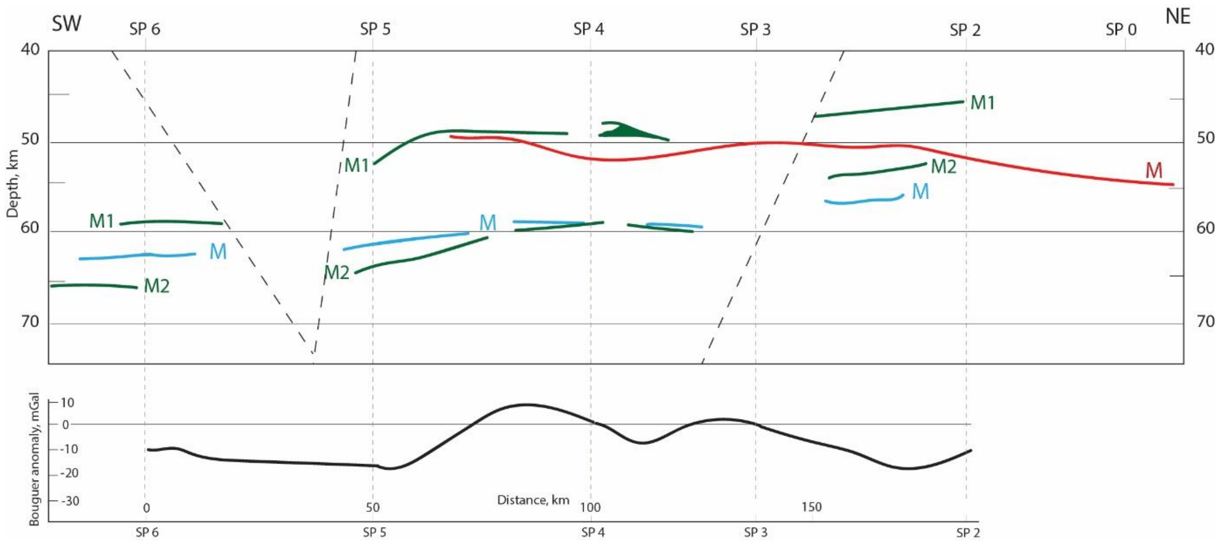

Figure 11. Sovetsk–Kohtla-Järve seismic sounding (DSS) profile. Moho transitional layer interpretation by Ankudinov et al. (1994) is shown in dark green (profiles M1 and M2). The blue line represents the modified Moho from All et al. (2004). The red line is Moho depth from this study. The lower panel shows the gravity profile from All et al. (2004).

The discrepancies between my findings and previous work may be due to differences in seismic velocity models used. In this study, I employed the University of Helsinki model (Tiira et al., 2022), which assumes that the Moho is at around 40 km depth, as the Vp exceeds 8.03 km/s beyond this depth. This model underestimates the Moho depth in Estonia, as the actual depth is closer to 50–60 km. I tested the impact of changing this velocity model at several stations by adjusting the depth ranges to 0–15 km, 15–55 km, and >55 km. These modifications suggest that the crust beneath Estonia may be 1–3 km thinner than indicated by the results of this study.

Another validation of the findings comes from comparing them with gravity data. I compared my data with two gravity maps (Figure 12). The thickened crust in northwest and western Estonia, and by the Russian station PUL, corresponds well with strong positive gravity anomalies. In northern Estonia, both gravity and Moho depth show less variation, which is consistent across datasets. This overall coherence between gravity anomalies and Moho depth trends suggests that the interpolated depth relief is geophysically reasonable. On the other hand, the gravity-based model by Solano-Acosta et al. (2023) shows noticeable differences, the cause of which is unclear and would require further investigation.

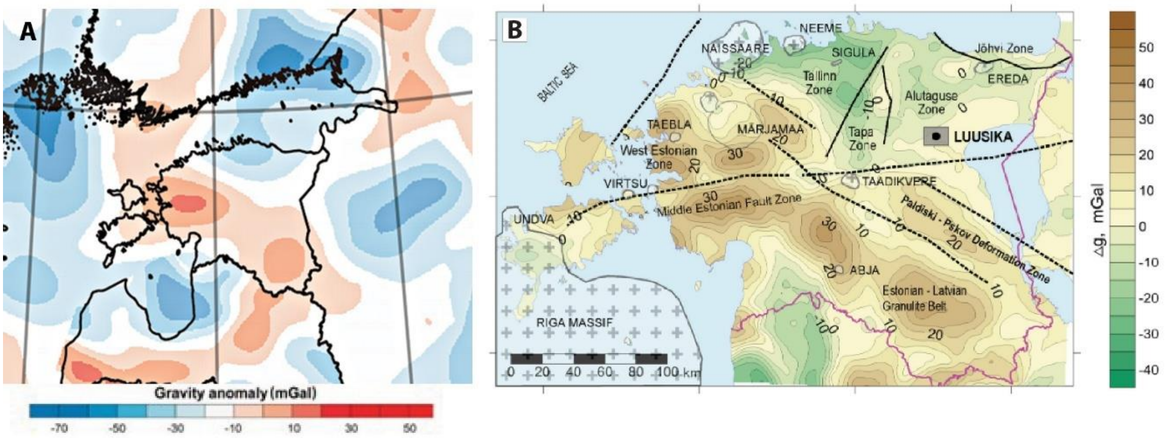

Figure 12. A) Filtered gravity data of Estonia and its surrounding areas (Zandersons & Karušs, 2020). B) Bouguer gravity map of Estonia (Dmitrijeva et al., 2018).

Comparisons with similar studies in Finland further support the validity of the results of my study. Alinaghi et al. (2003), used the same RF analysis, and observed similar patterns – thicker crust in southwest Finland (50–55 km) and thinner in southeast (40–45 km). The recent SOFIC profile study by Tiira et al. (2022) in southern Finland shows trends that also align with the current findings.

Further improvements of the study can be achieved through changing the seismic velocity model and incorporating other geophysical models. Further filtering of the RF data might be needed for noisy stations like SRPE, PISE, and EE04. Additional stations are needed in under-represented regions, such as southern Estonia and Latvia.

Conclusions

This study provides a new seismic perspective on the crustal structure beneath Estonia and surrounding regions by applying receiver function analysis to teleseismic data. Previous models of Moho depth in the area have relied heavily on gravimetric, magnetic, and sparse deep seismic sounding (DSS) data, often producing inconsistent results. By using data from both Estonian and nearby regional seismic stations, this study demonstrates that receiver function analysis can map crustal thickness in greater detail than previously possible.

The results reveal significant variation in Moho depth, ranging approximately from 48 km in southeastern Estonia and northern Latvia to 63 km in the northwestern Estonia. These findings are broadly consistent with earlier DSS profiles, as well as with gravity anomaly trends. In areas where comparisons were possible, results closely match previously found values – for example at the Vasula station.

While limitations remain due to the uneven distribution of seismic stations, particularly in southern Estonia, this study highlights the potential of receiver function method. As the seismic network continues to expand, future work will be able to improve spatial resolution. This study provides new and independent seismic insights to the lithospheric structure beneath Estonia and shows the importance of integrating seismological methods to regional geophysical studies.

Acknowledgements

I would like to express my gratitude to my supervisor, Heidi Soosalu, for her continuous support and guidance throughout the long process of writing this thesis. I am also thankful to my co-supervisor, Argo Jõeleht, for his insightful comments and helpful suggestions.

My thanks go to Tarmo All as well, for his engaging discussion and valuable input, and to Gennadi Baranov for his assistance in refining the figures. I am also grateful to Peter Makus for his support with the PyGLImER software, and to Kristo-Karl Aedma for sharing his previous work material.

References

Aedma, K. K. (2020). *Vastuvõtjafunktsiooni meetodi kasutamine ja Eesti maakoore paksuse hinnang Vasula seismojaamas registreeritud teleseismiliste maavärinate baasil* [Bakalaureusetöö, Tartu Ülikool]. http://hdl.handle.net/10062/69993

Alinaghi, A., Bock, G., Kind, R., Hanka, W., Wylegalla, TOR and SVEKALAPKO Working Groups (2003). Receiver function analysis of the crust and upper mantle from the North German Basin to the Archaean Baltic Shield. *Geophysical Journal International, 155*(2), 64–652. https://doi.org/10.1046/j.1365-246X.2003.02075.x

All, T., Puura, V., & Vaher, R. (2004). Orogenic structures of the Precambrian basement of Estonia as revealed from the integrated modelling of the crust. *Proc. Estonian Acad. Sci. Geol., 53*, 165–189. https://doi.org/10.3176/geol.2004.3.03

Ankudinov, S., Sadov, A., & Brio, H. (1994). Crustal structure of Baltic countries on the basis of deep seismic sounding data. *Proceedings of the Estonian Academy of Sciences. Geology*, *43*, 129–136. https://doi.org/10.3176/geol.1994.3.03

Backus, M. M., Cambois, G., Stoffa, P. L., Cary, P. W., Lorentz, G. A., Claerbout, J. F., Gibson, B., Larner, K. L., Goupillaud, P., Hale, I. D., Hargreaves, N. D., Calvert, A. J., Kjartansson, E., Levin, S. A., Lines, L. R., Treitel, S., Morley, L., Peacock, K. L., Ristow, D., ... & Yilmaz, O. (2001). Deconvolution. In O. Yilmaz (Ed.), *Seismic Data Analysis: Processing, Inversion, and Interpretation of Seismic Data* (Vol. 1, pp. 159–270). Society of Exploration Geophysicists. https://doi.org/10.1190/1.9781560801580.ch2

Beyreuther, M., Barsch, R., Krischer, L., Megies, T., Behr, Y., & Wassermann, J. (2010). ObsPy: A Python Toolbox for Seismology. *Electronic Seismologist.* https://doi.org/10.1785/gssrl.81.3.530

Bolt, B. A. (2003). *Earthquakes* (5th ed.). W. H. Freeman and Company.

Bormann, P., Engdahl, B., & Kind, R. (2012). *Seismic Wave Propagation and Earth models*. -In: Bormann, P. (Ed.), *New Manual of Seismological Observatory Practice 2 (NMSOP2)*. Potsdam: Deutsches GeoForschungsZentrum GFZ, 1–105. https://doi.org/10.2312/GFZ.NMSOP-2_ch2

Born, M., & Wolf, E. (1959). *Principles of optics: electromagnetic theory of propagation, interference and diffraction of light* (1st ed.). London; New York; Paris: Pergamon Press.

Castro-Artola, O., Iglesias, A., Schimmel, M., & Córdoba-Montiel, F. (2022). Moho reflections within seismic noise autocorrelations. *Journal of South American Earth Sciences, 120*, 104080. https://doi.org/10.1016/j.jsames.2022.104080

Chen, S., Shi, Y., Cao, B., Cao, S., Sun, Y., & Shi, W. (2024). Seismic deconvolution based on SNR-weighted stacking. *Journal of Applied Geophysics, 225*, 105380. https://doi.org/10.1016/j.jappgeo.2024.105380

Christensen, N. I., & Mooney, W. D. (1995). *Seismic velocity structure and composition of the continental crust: A global view*. JGR: Solid Earth, 100(B6), 9761–9788. https://doi.org/10.1029/95JB00259

Delph, J. R., Levander, A., & Niu, F. (2019). Constraining Crustal Properties Using Receiver Functions and the Autocorrelation of Earthquake-Generated Body Waves. *Journal of Geophysical Research, Solid Earth, 124*(8), 8981–8997. https://doi.org/10.1029/2019JB017929

Dmitrijeva M., Plado, J., & Oja, T. (2018). The Luusika potential field anomaly, eastern Estonia: modelling results. Proceedings of the Estonian Academy of Sciences. Geology, 67(4), 228–237. https://doi.org/10.3176/earth.2018.18

GEOFON Data Centre (1993). GEOFON Seismic Network. GFZ Data Services. Dataset/Seismic Network. https://doi.org/10.14470/TR560404

Geological Survey of Estonia (EGT) (1996). Estonian National Seismic Network (EESN). GFZ Data Services. Dataset/Seismic Network. https://doi.org/10.14470/RR425351

Grad, M., Tiira, T. and ESC Working Group (2009). The Moho depth map of the European Plate. *Geophysical Journal International, 176*(1), 279–292. https://doi.org/10.1111/j.1365-246X.2008.03919.x

Harland, K. E., White, R. S., & Soosalu, H. (2009). Crustal structure beneath the Faroe Islands from teleseismic receiver functions. *Geophysical Journal International, 177*(1), 115–124. https://doi.org/10.1111/j.1365-246X.2008.04018.x

Harris, C. R., Millman, K. J., van der Walt, S. J., Gommers, R., Virtanen, P., Cournapeau, D., ... & Oliphant, T. E. (2020). Array programming with NumPy. *Nature*, *585*(7825), 357–362. https://doi.org/10.1038/s41586-020-2649-2

He, P., Lei, J., Yuan, X., Xu, X., Xu, Q., Liu, Z., Qi, M., & Zhou, L. (2018). Lateral Moho variations and the geometry of the Main Himalayan Thrust beneath the Nepal Himalayan orogen revealed by teleseismic receiver functions. *Geophysical Journal International*, *214*, 1004–1017. https://doi.org/10.1093/gji/ggy192

Institute of Seismology, University of Helsinki. (1980). The Finnish National Seismic Network. GFZ Data Services. Dataset/Seismic Network. https://doi.org/10.14470/UR044600

Kaban, M.K., Sidorov, R.V., Soloviev, A.A., Gvishiani, A. D., Petrunin, A. G., Petrov, O. V., Kashubin, S. N., Androsov, E. A., & Milshtein, E. D. (2022). A New Moho Map for North-Eastern Eurasia Based on the Analysis of Various Geophysical Data. *Pure* *and Applied Geophysics, 179*, 3903–3916. https://doi.org/10.1007/s00024-021-02925-6

Langston, C. A. (1979). Structure under Mount Rainer, Washington, inferred from teleseismic body waves. *Journal of Geopghysical Research, 84,* 4749–4762. https://doi.org/10.1029/JB084iB09p04749

Makus, P., Rondenay, S., Sawade, L., Ottemöller, L., & Halpaap, F. (2021). PyGLImER: A New Modular Software Suite to Image Crustal and Upper-Mantle Discontinuities Using a Global Database of Ps and Sp Receiver Functions. *Authorea.* https://doi.org/10.1002/essoar.10506417.1

Matcharashvili, T., Chelidze, T., Javakhishvili, Z., Jorjiashvili, N., & Zhukova, N. (2012). Scaling features of ambient noise at different levels of local seismic activity: A case study for the Oni seismic station. *Acta Geophysica, 60,* 809–832. https://doi.org/10.2478/s11600-012-0006-z

Mohorovičić, A. (1910). Earthquake of 8 October 1909. *Reprinted in Geofizika, 9,* 3–55.

Mondol, N. H. (2010). Seismic Exploration. *Petroleum Geoscience,* 375–402. Springer. https://doi.org/10.1007/978-3-642-02332-3_17

Nanometrics Inc. (2009). Trillium 120P/PA seismometer user guide. (15149R6). Nanometrics, Inc, Kanata. https://jssp.wustl.edu/manuals/sensor/Trillium120P-PA_UserGuide.pdf

Quinteros, J., Carter, J. A., Schaeffer, J., Trabant, C., & Pedersen, H. A. (2021b). Exploring Approaches for Large Data in Seismology: User and Data Repository Perspectives. *Seismological Research Letters, 92*(3), 1531–1540. https://doi.org/10.1785/0220200390

Quinteros, J., Strollo, A., Evans, P. L., Hanka, W., Heinloo, A., Hemmleb, S., Hillmann, L., Jaeckel, K-H., Kind, R., Saul, J., Zieke, T., & Tilmann, F. (2021a). The GEOFON Program in 2020. *Seismological Research Letters, 92*(3), 1610–1622. https://doi.org/10.1785/0220200415

Ravikumar, C. S., Ramasamy, V., & Thandavamoorthy, T. S. (2014). Mechanism of Earthquake and Damages of Structures. *International Journal of Current Enginering and Technology, 4*(2), 820–825. https://inpressco.com/wp-content/uploads/2014/04/Paper67820-825.pdf

Ringler, A. T., & Evans, J. R. (2015). A Quick SEED Tutorial. *Seismological Research Letters, 86*(6), 1717–1725. https://doi.org/10.1785/0220150043

Saygin, E. (2007). Seismic Receiver and Noise Correlation Based Studies in Australia. [PhD thesis. The Australian National University]. https://doi.org/10.25911/5d7a2d1296f96

Shearer, P. M. (1999). *Introduction to Seismology*. Cambridge University Press.

Shuey, R. T. (1985). A simplification of the Zoeppritz equations. *Geophysics*. https://doi.org/10.1190/1.1441936

Sildvee, H., & Vaher, R. (1995). Geologic structure and seismic activity of Estonia. *Proc. Estonian Acad. Sci. Geol., 44*, 15–25. https://doi.org/10.3176/geol.1995.1.02

Solano-Acosta, J. D., Soesoo, A., & Hints, R. (2023). New insights of the crustal structure across Estonia using satellite potential fields derived from WGM-2012 gravity data and EMAG2v3 magnetic data. *Tectonophysics, 846,* 229656. https://doi.org/10.1016/j.tecto.2022.229656

Soosalu, H. (2024). Seismiline seire. Aruanne riikliku keskkonnaseire allprogrammi „Seismiline seire" täitmisest 2023. aastal. *Eesti Geoloogiateenistus.* https://fond.egt.ee/fond/egf/9836

Soosalu, H. (2025). Seismiline seire. Aruanne riikliku keskkonnaseire allprogrammi „Seismiline seire" täitmisest 2024. aastal. *Eesti Geoloogiateenistus.* https://fond.egt.ee/fond/egf/9948

Tiira, T., Janik, T., Veikkolainen, T., Komminaho, K., Skrzynik, T., Väkevä, S., & Heinonen, A. (2022). Implications on crustal structure from the South Finland Coastal (SOFIC) deep seismic sounding profile. *Bulletin of the Geological Society of Finland, 94*(2), 165–180. https://doi.org/10.17741/bgsf/94.2.004

Tšugai, A. (2010). *Eestis registreeritud kauged maavärinad* [Magistritöö, Tartu Ülikool].

Zandersons, V., & Karušs, J. (2020). Gravity-derived Moho map for Latvia. *Estonian Journal of Earth Sciences*, *69*, 177–188. https://doi.org/10.3176/earth.2020.19

Zoeppritz equations. (25.12.2024). *Wikipedia.* https://en.wikipedia.org/w/index.php?title=Zoeppritz_equations&oldid=1265166819

Appendices

Appendix 1. The used seismic stations

Station name	Coordinates (˚N; ˚E)	Location
ARBE	59.4365; 25.98410	Estonia, Lääne-Virumaa, Arbavere Research Center
EE04	59.374; 27.875	Estonia, Ida-Virumaa, Vaivara
EE06	58.9695; 22.8482	Estonia, Hiiumaa, Soera Museum
MEF	60.21719; 24.39581	Finland, Metsähovi Geodetic Research Station
MTSE	58.7144; 23.8146	Estonia, Pärnumaa, Matsalu National Park Visitor Center
NOPE	59.2089; 23.6238	Estonia, Läänemaa, Nõva RMK Visitor Center
PISE	57.8414; 27.4674	Estonia, Võrumaa, Piusa Caves
PLDE	59.3481; 24.074	Estonia, Harjumaa, Paldiski
PUL	59.7728; 30.3222	Russia, Pulkovskoye Observatory
PVF	60.5453; 25.859	Finland, Övre Rikeby, Pernaja
SLIT	57.6287; 22.2905	Latvia, Dudanga, Slīteres
SRGE	58.6563; 25.2425	Estonia, Pärnumaa, TalTech Särghaua Earth Science Center
SRPE	59.46331; 24.380	Estonia, Harjumaa, Suurupi
TOSE	58.8728; 26.2728	Estonia, Jõgevamaa, Tooma Weather Station
TRTE	58.3786; 26.7205	Estonia, Tartumaa, Tartu Old Observatory
VJF	60.5388; 27.555	Finland, Virolahti, Virojoki
VSU	58.462; 26.73469	Estonia, Tartumaa, Vasula

Appendix 2. RF figures of SRGE and TOSE

A

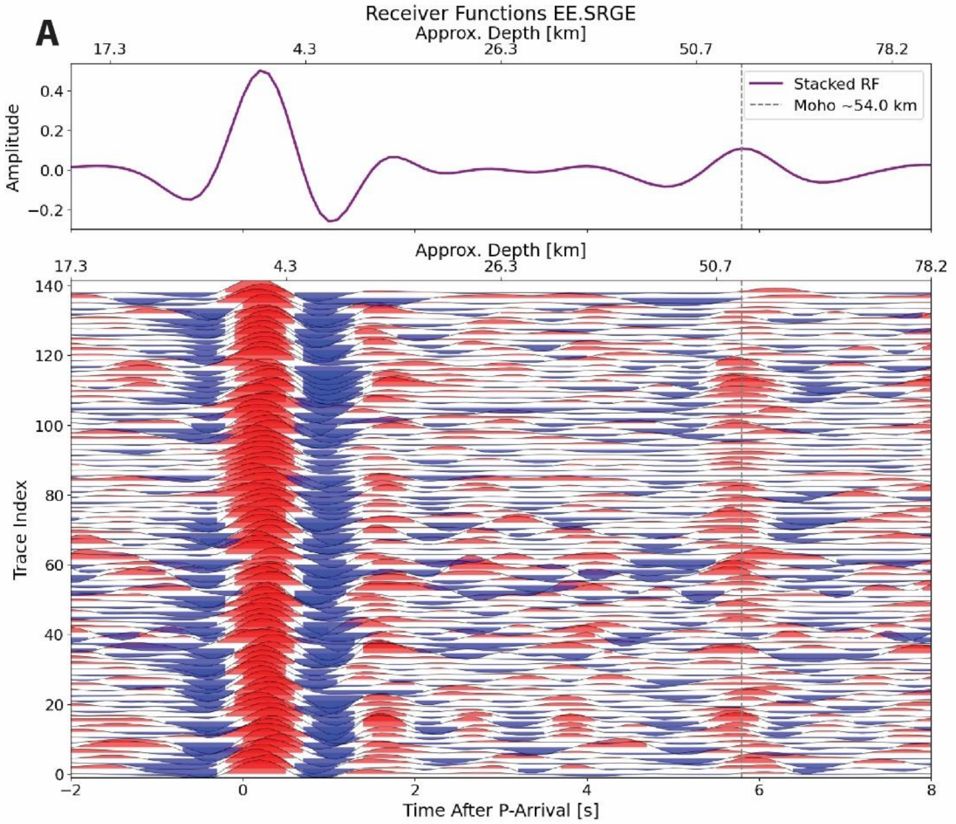

B

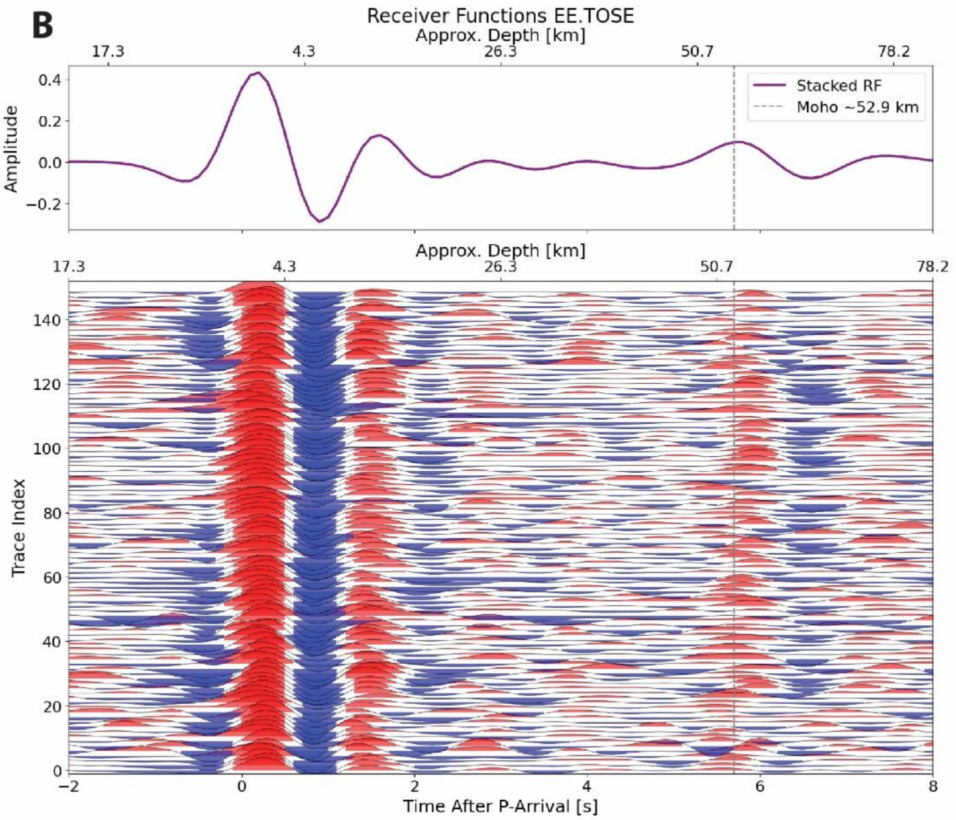

Lisa
rektori 07.04.2020 käskkirjale nr 1-8/17

Lihtlitsents lõputöö reprodutseerimiseks ja lõputöö üldsusele kättesaadavaks tegemiseks[1]

Mina Sonja Kõrvits

1. Annan Tallinna Tehnikaülikoolile tasuta loa (lihtlitsentsi) enda loodud teose
Crustal thickness of Estonia: a receiver function analysis,

mille juhendaja on Heidi Elisabeth Soosalu,

1.1 reprodutseerimiseks lõputöö säilitamise ja elektroonse avaldamise eesmärgil, sh Tallinna Tehnikaülikooli raamatukogu digikogusse lisamise eesmärgil kuni autoriõiguse kehtivuse tähtaja lõppemiseni;

1.2 üldsusele kättesaadavaks tegemiseks Tallinna Tehnikaülikooli veebikeskkonna kaudu, sealhulgas Tallinna Tehnikaülikooli raamatukogu digikogu kaudu kuni autoriõiguse kehtivuse tähtaja lõppemiseni.

2. Olen teadlik, et käesoleva lihtlitsentsi punktis 1 nimetatud õigused jäävad alles ka autorile.

3. Kinnitan, et lihtlitsentsi andmisega ei rikuta teiste isikute intellektuaalomandi ega isikuandmete kaitse seadusest ning muudest õigusaktidest tulenevaid õigusi.

28.05.2025

(*allkirjastatud digitaalselt*)

[1] *Lihtlitsents ei kehti juurdepääsupiirangu kehtivuse ajal vastavalt üliõpilase taotlusele lõputööle juurdepääsupiirangu kehtestamiseks, mis on allkirjastatud teaduskonna dekaani poolt, välja arvatud ülikooli õigus lõputööd reprodutseerida üksnes säilitamise eesmärgil. Kui lõputöö on loonud kaks või enam isikut oma ühise loomingulise tegevusega ning lõputöö kaas- või ühisautor(id) ei ole andnud lõputööd kaitsvale üliõpilasele kindlaksmääratud tähtajaks nõusolekut lõputöö reprodutseerimiseks ja avalikustamiseks vastavalt lihtlitsentsi punktidele 1.1. jq 1.2, siis lihtlitsents nimetatud tähtaja jooksul ei kehti.*